Eur. Phys. J. A (2020) 56:162
https://doi.org/10.1140/epja/s10050-020-00147-3

THE EUROPEAN PHYSICAL JOURNAL A

Regular Article - Theoretical Physics

On the excitation of the 2_1^+ state in ^{12}C in the $(e, e'\gamma)$ reaction

D. H. Jakubassa-Amundsen[1], **V. Yu. Ponomarev**[2,a]

[1] Mathematics Institute, University of Munich, Theresienstrasse 39, 80333 Munich, Germany
[2] Institute of Nuclear Physics, Technical University of Darmstadt, 64289 Darmstadt, Germany

Received: 7 February 2020 / Accepted: 9 April 2020 / Published online: 5 June 2020

Communicated by Pierre Capel

Abstract The excitation of the carbon 2^+ state at 4.439 MeV by 70−150 MeV electron impact and its subsequent decay to the ground state by photon emission is described within the distorted-wave Born approximation. The transition densities are obtained from the nuclear quasiparticle phonon model. The photon angular distributions are compared with earlier results and with experiment, including the influence of bremsstrahlung. Predictions for spin asymmetries in the case of polarized electron impact are also made.

1 Introduction

With the advent of modern accelerators and efficient spin-polarized electron sources, such as the Darmstadt facility S-DALINAC, coincidence measurements between electrons scattered inelastically from nuclei and decay photons are feasible with high accuracy. This has stimulated the theoretical reinvestigation of the lowest quadrupole excitation of ^{12}C by electron impact which had been studied in a pioneer coincidence experiment by Papanicolas et al. [1], followed by a theoretical interpretation by Ravenhall et al. [2].

Nuclear excitation by electron impact is a powerful tool to obtain nuclear structure information [3,4], because only the electromagnetic interaction between the participating particles is involved. The nuclear properties enter exclusively into the electric and magnetic transition densities ϱ_L and $J_{L,L\pm1}$. They can be calculated from nuclear models.

The first theoretical investigation of the coincident nuclear excitation and decay (ExDec) process dates back to Hubbard and Rose [5], who employed the plane-wave Born approximation (PWBA). This theory was subsequently applied to the 2_1^+ excitation of ^{12}C [6]. Later, a combination of the distorted-wave Born approximation (DWBA) for the electric transition and the PWBA for the magnetic transition was used [2]. In these calculations, the nuclear transition densities were taken in the form of Fourier-Bessel series with coefficients obtained from a fit to early measurements of inclusive electron scattering form factors (e.g. [7,8]). It has been demonstrated that the current transition densities $J_{L,L\pm1}$ are very strong for the ^{12}C nucleus, such that interference phenomena between electric and magnetic excitations are already visible at scattering angles in the forward hemisphere where the cross sections are large. Such interference effects, augmented in coincidence experiments, are particularly sensitive to details of the nuclear structure.

A competitive process to ExDec is the emission of bremsstrahlung, which contributes coherently to the photon emission from nuclear decay to the ground state [5]. Bremsstrahlung calculations at high collision energies are usually performed within the relativistic PWBA. Since ^{12}C is a spin-zero nucleus, only potential scattering has to be taken into account [9]. For the radiation of photons with small frequencies as compared to the collision energy (i.e. for low momentum transfer), it was shown by Bethe and Maximon [10] that the PWBA, as limiting case of the Sommerfeld-Maue theory, is an appropriate theory, irrespective of the nuclear charge.

Bremsstrahlung may have a considerable influence on the angular distribution of the emitted photons, and was already taken into account in [6], however not in the ^{12}C investigation by Ravenhall et al. [2]. More recently, when studying the 2_1^+ and 2_2^+ excitations in the $(e, e'\gamma)^{92}$Zr reaction [11], it was shown that the contribution of bremsstrahlung to the detected photons depends not only on the scattering angle, but also on the resolution of the photon detector, which in general is much poorer than the line width of the decay photon.

Within a new campaign of the coincidence experiments in the $(e, e'\gamma)$ reaction at S-DALINAC [12], it is planned to revisit the previous measurements in [1] to test the set-up. In the present paper, we extend the theoretical analysis for this experiment. We employ a full DWBA prescription

[a] e-mail: ponomare@theorie.ikp.physik.tu-darmstadt.de (corresponding author)

of the ExDec process and add bremsstrahlung coherently. This guarantees a consistent representation of all interference effects, which are absent in PWBA. We will use the charge and current transition densities from [2] and also the ones from the random phase approximation of the quasiparticle phonon model (QPM [13,14]) to discuss the nuclear structure effects on the ExDec cross sections. Section 2 provides the differential cross section results. We also compare with results where the QPM transition densities are replaced by the ones fitted to experiment. Section 3 deals with the Sherman function for polarized electrons. A short conclusion is given in Sect. 4. Atomic units ($\hbar = m = e = 1$) are used unless indicated otherwise.

2 Cross section for the ExDec process

The triply differential cross section for the inelastic scattering of an unpolarized electron with (total) initial energy E_i and final energy E_f into the solid angle $d\Omega_f$ with the simultaneous emission of a photon with frequency ω into the solid angle $d\Omega_k$ is given by [5,11]

$$\frac{d^3\sigma}{d\omega d\Omega_k d\Omega_f} = \frac{2\pi^2\omega^2 E_i E_f k_f}{k_i c^7 f_{\rm rec}} \sum_{\sigma_i,\sigma_f} \times \sum_{\lambda} \left| M_{fi}^{(1)} + M_{fi}^{(2)} + M_{fi}^{\rm brems} \right|^2, \quad (2.1)$$

where $\boldsymbol{k}_i$ and $\boldsymbol{k}_f$ are, respectively, the electron momenta in initial and final state. Here we have assumed that polarization is not observed, such that (2.1) includes a sum over the photon polarization $\boldsymbol{\epsilon}_\lambda$ and over the final electron spin projection σ_f, in addition to an average over the initial-state spin projection σ_i. Furthermore, it is assumed that a spin-zero nucleus decays into its ground state, so that no further spin degrees of freedom are present. The factor $f_{\rm rec}$ is due to the kinematical recoil arising from the finite mass of the nucleus.

The amplitude $M_{fi}^{(1)}$ describes the excitation of the nucleus into a quadrupole state n with energy E_x, spin $J_n = 2$ and magnetic quantum number M_n, followed by radioactive decay according to the decay width Γ_n,

$$M_{fi}^{(1)} = i \frac{Z_T c^2}{4\pi\sqrt{\omega}} \frac{1}{\omega - E_x + i\Gamma_n/2} \times \sum_{M_n=-J_n}^{J_n} A_{ni}^{\rm exc}(M_n)\, A_{fn}^{\rm dec}(M_n), \quad (2.2)$$

where Z_T is the nuclear charge number and $A_{ni}^{\rm exc}$ and $A_{fn}^{\rm dec}$ are, respectively, the excitation and decay amplitudes as e.g. given in [11].

The second transition amplitude in (2.1), $M_{fi}^{(2)}$, describes the reversed process where the photon emission occurs before the nuclear excitation. The basic difference to $M_{fi}^{(1)}$ is a resonance denominator given by $\omega + E_x + i\Gamma_n/2$ [11]. Due to the smallness of Γ_n as compared to E_x, this reversed process is suppressed by many orders of magnitude for the present choice $\omega = E_x$. Even for ω differing from E_x by the detector resolution (assumed to be 3%), $M_{fi}^{(2)}$ is not more than one percent of $M_{fi}^{(1)}$. Therefore this process is disregarded.

The last term in (2.1), $M_{fi}^{\rm brems}$, is the contribution from bremsstrahlung photons with the same frequency ω,

$$M_{fi}^{\rm brems} = i \frac{c}{\sqrt{\omega}} \int d\boldsymbol{x}\, \psi_f^{(\sigma_f)+}(\boldsymbol{x})\, (\boldsymbol{\alpha}\boldsymbol{\epsilon}_\lambda^*)\, e^{-i\boldsymbol{k}\boldsymbol{x}}\, \psi_i^{(\sigma_i)}(\boldsymbol{x}), \quad (2.3)$$

where ψ_i and ψ_f are, respectively, the initial and final scattering states of the electron, while $\boldsymbol{k}$ is the photon momentum and $\boldsymbol{\alpha}$ is a vector of Dirac matrices. In the PWBA, when ψ_i and ψ_f are expanded in terms of plane waves, the rhs of (2.3) has to be multiplied by the Dirac form factor $F_1(q)$, which accounts for the charge distribution of the nucleus [15,16].

2.1 Nuclear excitation

The excitation amplitude $A_{ni}^{\rm exc}$ is conventionally calculated with the help of partial-wave expansions [17,18]. It is composed of the contributions originating from the electric transition density $\varrho_L(x_N)$ and the magnetic transition densities $J_{L,L\pm1}(x_N)$ with $L = 2$. Their dependence on the nuclear coordinate x_N is displayed in Fig. 1, where the magnetization current densities contributing to J_{23} and J_{21} are shown separately. The transition densities, calculated within the QPM, are presented by solid lines. They have been calculated within the one-phonon approximation by adjusting the strength of the residual interaction to reproduce the experimental value of the $B(E2, g.s. \to 2_1^+) = 39.7\ {\rm e}^2{\rm fm}^4$ [19]. Notice that the QPM transition densities deviate considerably from those provided in [2] which are obtained from a Fourier-Bessel fit to scattering experiments. The $B(E2, g.s. \to 2_1^+)$ value obtained from the integration of the charge transition density [4],

$$B(E2, g.s. \to 2^+) = 5 \left| \int_0^\infty r^4 \varrho_2(r) dr \right|^2, \quad (2.4)$$

when using ϱ_2 from [2], equals to $42.41\ {\rm e}^2{\rm fm}^4$, which is 7% above the experimental value. A stronger peak at the surface of the charge transition density [2] is compensated by a slightly stronger tail of the QPM density.

For quadrupole excitation there are five magnetic sublevels M_n, which are populated with a probability given by

$$P(M_n) = \frac{d\sigma^{\rm exc}/d\Omega_f(M_n)}{(d\sigma^{\rm exc}/d\Omega_f)_{\rm tot}}, \quad (2.5)$$

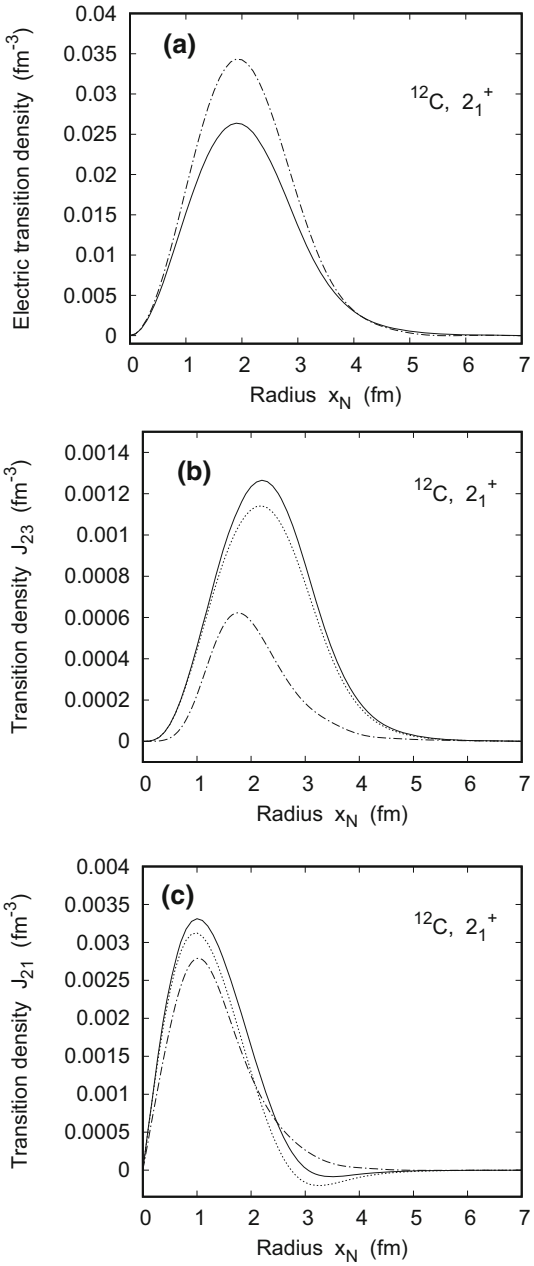

Fig. 1 Transition densities **a** ϱ_2, **b** J_{23} and **c** J_{21} for the 2_1^+ excitation of ^{12}C at 4.439 MeV as a function of x_N. Full line – QPM calculations (consisting in **b** and **c** of magnetization and convection currents). Dotted line – Contribution of the magnetization current to J_{23} and J_{21}. Also shown are the transition densities of Ravenhall et al. (dash-dotted line): ϱ_2 and J_{23} are taken from [2], J_{21} is obtained from the continuity equation [4]; note, however, the reversed sign of J_{21} as compared to the definition in [4]

where (see, e.g. [20])

$$\frac{d\sigma^{\rm exc}}{d\Omega_f}(M_n) = \frac{2\pi^3 E_i E_f k_f}{k_i c^2\ \tilde{f}_{\rm rec}} \sum_{\sigma_i,\sigma_f}$$

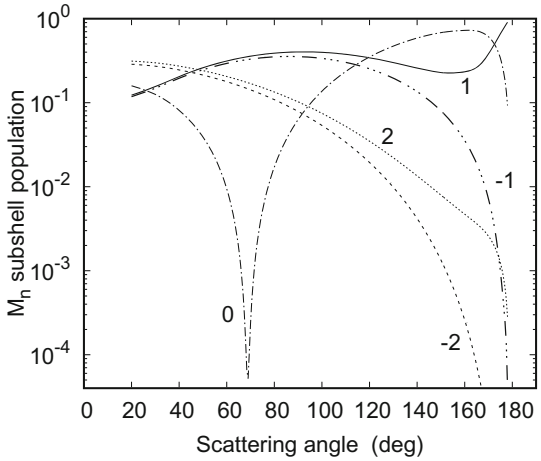

Fig. 2 Subshell population probabilities $P(M_n)$ for the 2_1^+ excitation of ^{12}C by 70 MeV electrons as a function of scattering angle ϑ_f. Dash-dotted line – $M_n = 0$; full line – $M_n = 1$; dotted line – $M_n = 2$; triple dash-dotted line – $M_n = -1$; dashed line – $M_n = -2$. The probabilities sum up to unity

$$\times \sum_{M_n'=-2}^{2} \left|A_{ni}^{\rm exc}(M_n')\right|^2\ \delta_{M_n,M_n'}, \qquad (2.6)$$

valid for spin-zero nuclei. The recoil denominator $\tilde{f}_{\rm rec}$ differs from $f_{\rm rec}$ in (2.1) due to E_x in the energy balance. The total excitation cross section in the denominator of (2.5) results from (2.6) with the delta function removed.

The calculation of the exact electronic scattering states by means of the Dirac equation is performed with the help of the Fortran code RADIAL by Salvat et al. [21]. The nuclear potential of ^{12}C is generated from the Fourier-Bessel expansion of the ground-state charge distribution [22]. The radial integrals in the transition matrix elements are evaluated by means of the complex-plane rotation method (CRM) introduced in [23] and applied to electron scattering in [24].

The M_n-sublevel populations for a collision energy of 70 MeV as a function of scattering angle ϑ_f are displayed in Fig. 2. It is seen that at scattering angles below 40° all levels have similar occupation probabilities, in particular the pairs $(+M_n, -M_n)$. However, in the backward hemisphere, it is just $M_n = 0$ and $M_n = 1$ which remain important, $M_n = 1$ taking over for $\vartheta_f \to 180°$. This is due to the strong influence of the magnetic transitions at small electron–nucleus distances (corresponding to a large momentum transfer, respectively to large scattering angles).

2.2 Decay of the excited nucleus

In all subsequent results, a coplanar geometry is chosen, where the photon is emitted in the scattering plane, spanned by $\boldsymbol{k}_i$ (which is taken as z-axis) and $\boldsymbol{k}_f$. Thus the azimuthal angle φ between $\boldsymbol{k}_i$ and $\boldsymbol{k}_f$ is 0° or 180°.

For the carbon 2_1^+ state at $E_x = 4.439$ MeV, the ground-state decay width is $\Gamma_n = (1.08 \pm 0.06) \times 10^{-2}$ eV [25]. The ground-state decay amplitude $A_{fn}^{\rm dec}$ is mediated solely by the current transition densities $J_{L,L\pm1}$ from Fig. 1b, c. According to the different occupation probabilities of the M_n-substates, the intensity of the emitted decay photons depends on M_n as well. Figure 3 shows the triply differential cross section for the excitation of the M_n-subshell and its subsequent decay, defined according to (2.1) by

$$\frac{d^3\sigma}{d\omega d\Omega_k d\Omega_f}(M_n) = \frac{2\pi^2\omega^2 E_i E_f k_f}{k_i c^7 \; f_{\rm rec}} \times \sum_{\sigma_i,\sigma_f} \sum_{\lambda} \left| M_{fi}^{(1)}(M_n) \right|^2 , \qquad (2.7)$$

where $M_{fi}^{(1)}(M_n)$ is obtained from (2.2) if the sum over M_n is dropped, corresponding to the excitation of just one substate M_n. In that case, the photon angular distribution is symmetric with respect to $\theta_k = 180°$ and is a superposition of dipole and quadrupole patterns [11]. This symmetry is lost in the total cross section where all M_n subshells are added coherently. In particular, there are angles θ_k where the total cross section is well below any M_n-subshell cross section (for a scattering angle of $\vartheta_f = 80°$ near e.g. $\theta_k = 40°$, see Fig. 3a). At backward angles (Fig. 3b), the total cross section is mainly composed of the $M_n = 0$ and $M_n = 1$ contributions according to the occupation probabilities from Fig. 2.

In order to display the importance of electric and magnetic excitation, Fig. 4 shows the contributions from potential scattering (arising from ϱ_2) and from magnetic scattering (due to J_{23}, J_{21}) entering into the excitation amplitude $A_{ni}^{\rm exc}$. Of course, the decay amplitude $A_{fn}^{\rm dec}$ is kept unchanged in both cases. In the forward hemisphere, even up to scattering angles $\vartheta_f \sim 160°$, the excitation by the electric force is largely dominant at all photon angles (Fig. 4a). Only a little shift of the minima to smaller θ_k is observed when the excitation by the current interaction is included. Coulomb distortion effects, measured by means of the difference between the DWBA and the PWBA results, can basically be neglected for light nuclei such as ^{12}C for not too large scattering angles. We also note that at 140° the photon angular distribution has still the same regular quadrupole pattern as for the smaller angle 80° from Fig. 3a. At the backmost angles (Fig. 4b for 175°), the magnetic scattering gives an essential contribution to the cross section, which modulates the quadrupole pattern considerably. This leads to a shift of the minima by about 20° as compared to potential scattering. Also the Coulomb distortion effects are considerably larger, up to 10 percent.

In Fig. 5a the DWBA results from the QPM densities are compared with those based on the Ravenhall et al. [2] densities included in Fig. 1. At the parameters of the measurements [1], a collision energy of 66.9 MeV and a scattering angle of 80°, the Ravenhall cross section is enhanced by a factor of

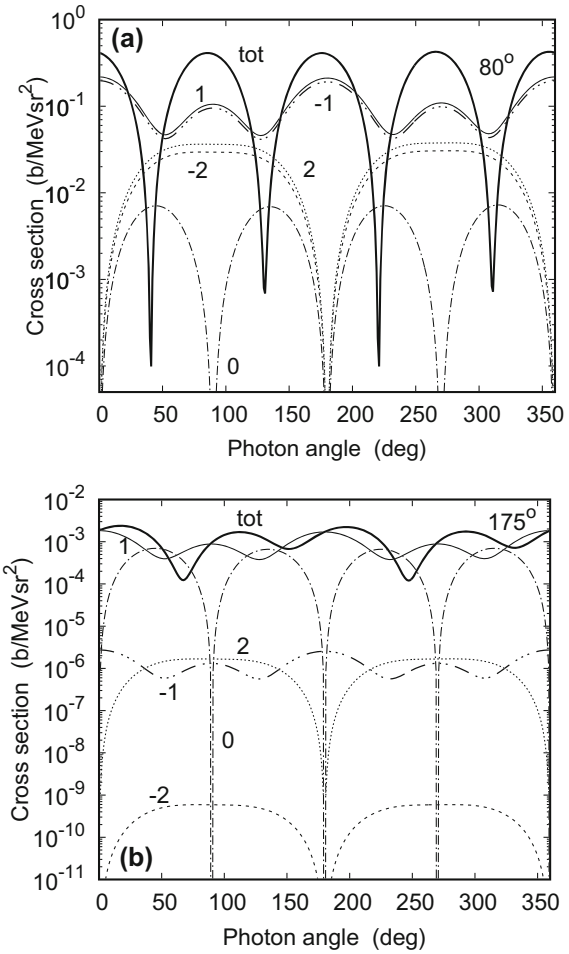

Fig. 3 M_n-subshell cross sections $\frac{d^3\sigma}{d\omega d\Omega_k d\Omega_f}(M_n)$ for the 2_1^+ excitation of ^{12}C by 70 MeV electrons and subsequent decay for scattering angles **a** $\vartheta_f = 80°$ and **b** $\vartheta_f = 175°$, with azimuthal angle $\varphi = 0$ between electron and photon, as a function of photon angle θ_k. Dash-dotted line – $M_n = 0$; full line – $M_n = 1$; dotted line – $M_n = 2$; triple dash-dotted line – $M_n = -1$; dash-dotted line – $M_n = -2$. Also shown is their coherent sum, the total cross section (thick solid line)

3.5. This results from the higher transition density ϱ_2, since electric excitation is dominating at this angle. Included in the figure are results for potential scattering within the PWBA, where one of the minima in the photon angular distribution coincides with the angle θ_q which the momentum transfer $\boldsymbol{q} = \boldsymbol{k}_i - \boldsymbol{k}_f$ forms with the z-axis ($\theta_q = 312.5°$). This results in an angular distribution which is azimuthally symmetric with respect to θ_q [2]. The shift between the minima of the electric PWBA and the full DWBA is about 2°, which is verified by the experimental data [1]. These data are measured on a relative scale and are in Fig. 5a normalized to the respective theories. It follows from Fig. 4a that the shift in angle is basically due to magnetic scattering and not to distortion effects. In Fig. 5b the scattering angle is increased to 170°. At this angle, the maxima of the Ravenhall results do not coincide anymore with those from the QPM

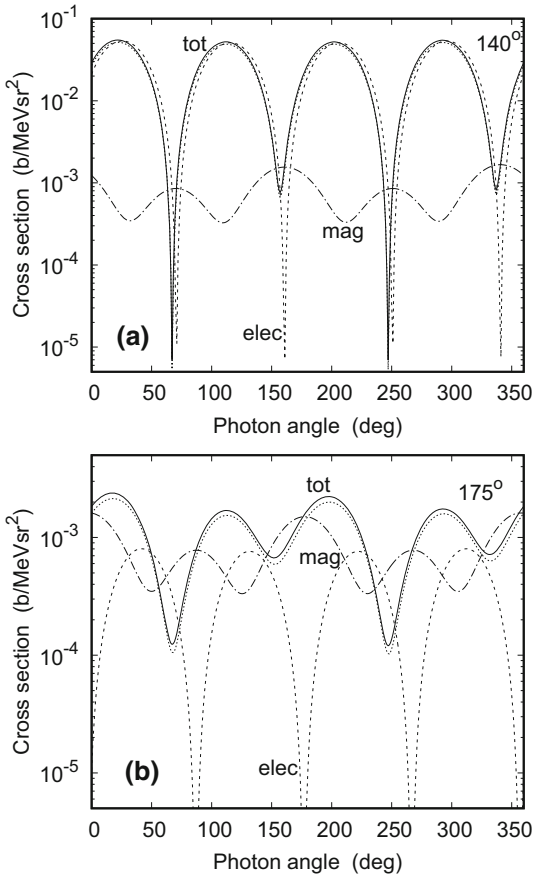

Fig. 4 Triply differential cross section for the nuclear ExDec process of the ^{12}C, 2^+_1 state by 70 MeV electrons **a** at $\vartheta_f = 140°$ and **b** at $\vartheta_f = 175°$, with $\varphi = 0$, as a function of photon angle θ_k. Total cross section: full line – DWBA; dotted line – PWBA. Also shown are the DWBA electric contribution (dashed line) and magnetic contribution (dash-dotted line) to the total cross section

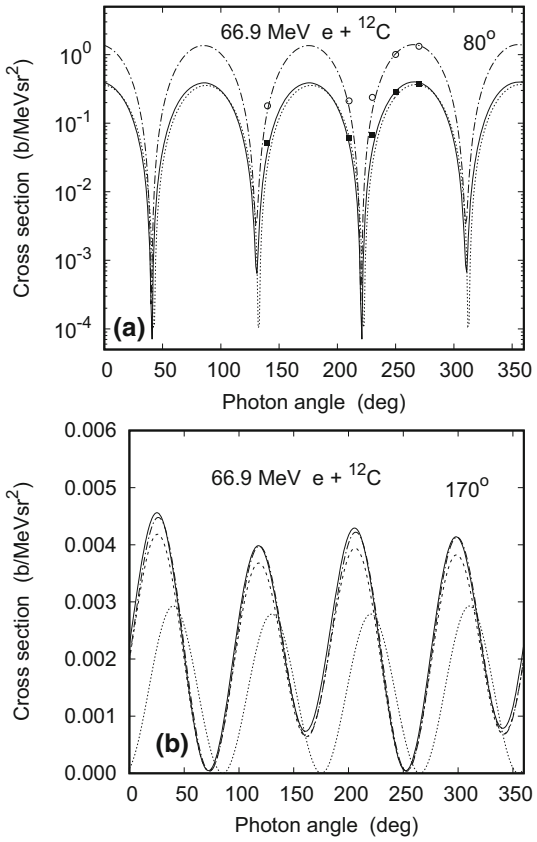

Fig. 5 Triply differential cross section for the nuclear ExDec process of the ^{12}C, 2^+_1 state by 66.9 MeV electron impact at **a** $\vartheta_f = 80°$ and **b** $\vartheta_f = 170°$, with $\varphi = 0$, as a function of photon angle θ_k. Full line – DWBA results; dashed line – PWBA results (in **b**); dotted line – PWBA results for electric excitation (all with QPM densities); dash-dotted line – DWBA results with Ravenhall densities. In **b**, the Ravenhall results are scaled down by a factor of 0.27 to display the differences in shape. The experimental data (open circle) in **a** are taken from Papanicolas et al. [1]. The same data (blacksquare) are scaled down by a factor of 0.285 to fit the QPM results

densities. Although the importance of potential scattering has decreased, the Ravenhall cross sections are still a factor of 3.7 above the QPM ones. This may be caused by an enhanced current J_{21} near the surface of the nucleus. Note that the nuclear radius of ^{12}C is $R_N = 1.2\ A^{1/3} = 2.75$ fm, which has to be compared to the distance of closest approach during the electron-nucleus encounter, determined by the inverse momentum transfer ($q^{-1} = 1.53$ fm for 66.9 MeV and 170°). We note that the QPM current densities do not include two-body currents as the ones of Ravenhall extracted from the data. It has been demonstrated recently that two-body currents substantially influence the transversal electromagnetic response of ^{12}C at high q-values [26]. Whether we are dealing with the same kind of effect at low q requires special studies.

2.3 Influence of bremsstrahlung

In order to give predictions for the contribution of bremsstrahlung to the nuclear ExDec process it is important to account for the finite resolution $\Delta\omega$ of the photon detector. As far as the nuclear ExDec process with its resonant behaviour is concerned, the averaging over the detector resolution leads basically to a reduction of intensity, but not to a change in the photon angular distribution. Bremsstrahlung, on the other hand, due to its weak dependence on ω, is hardly affected by the averaging procedure. When both contributions are considered, the averaged photon intensity at the peak frequency $\omega = E_x$ is calculated from

$$\left\langle \frac{d^3\sigma}{d\omega d\Omega_k d\Omega_f} \right\rangle_{\Delta\omega} \approx \frac{2\pi^2 E_i}{k_i c^7} \sum_{\sigma_i,\sigma_f} \sum_{\lambda} \times \frac{1}{\Delta\omega} \int_{E_x-\frac{\Delta\omega}{2}}^{E_x+\frac{\Delta\omega}{2}} d\omega' \, \frac{\omega'^2 E_f k_f}{f_{\rm rec}} \times \left| M_{fi}^{(1)} + M_{fi}^{\rm brems} \right|^2 , \quad (2.8)$$

such that the different ω-behaviour of $M_{fi}^{(1)}$ and $M_{fi}^{\rm brems}$ leads to a change in the θ_k-distribution which strongly depends on

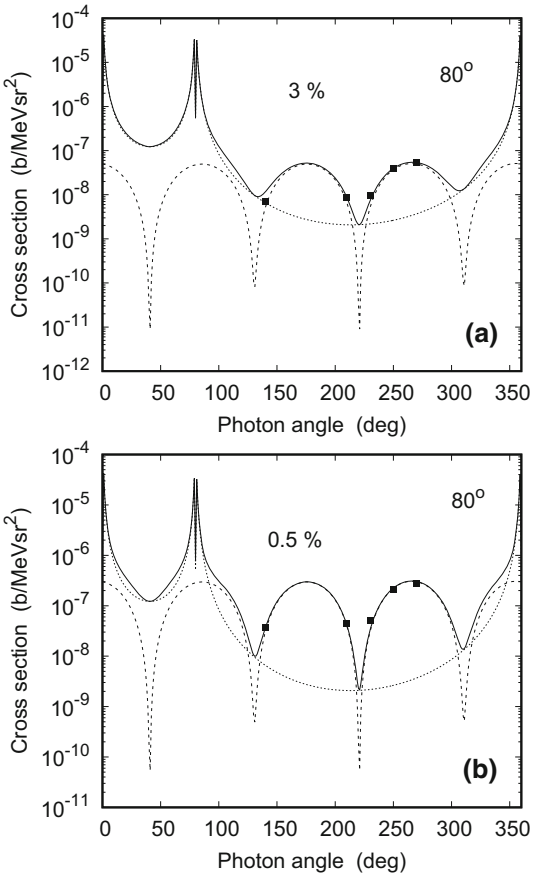

Fig. 6 Averaged triply differential cross section for the coincident $(e, e'\gamma)$ process by 66.9 MeV electrons scattered at $\vartheta_f = 80°$, with $\varphi = 0$, as a function of photon angle θ_k. The detector resolution is **a** $\Delta\omega/\omega = 3\%$ (corresponding to $\Delta\omega = 133$ keV), and **b** $\Delta\omega/\omega = 0.5\%$ (corresponding to $\Delta\omega = 22.2$ keV). dashed line – photons from the nuclear ExDec process; dotted line – bremsstrahlung; full line – coherent sum. The experimental data (blacksquare) are from Papanicolas et al. [1] and are normalized to the full lines

$\Delta\omega$. This feature is displayed in Fig. 6a where a resolution of $\Delta\omega/\omega = 3\%$ is taken, corresponding to a LaBr photon detector to be used in experiments, while in Fig. 6b, $\Delta\omega/\omega = 0.5\%$ is assumed. Again, the experimental parameters, $E_e = E_i - c^2 = 66.9$ MeV, the scattering angle $\vartheta_f = 80°$ and $\omega = 4.439$ MeV, have been chosen. The bremsstrahlung angular distribution is characterized by the narrow double-peak structure near $\theta_k = 0$ and near $\theta_k = \vartheta_f$ for $\omega \ll E_e$. These structures dominate the photon distribution from the ExDec process. In addition, the bremsstrahlung photons fill the minima of the quadrupole pattern, the more so, the poorer the detector resolution. We note that the experimental data points are slightly better reproduced with a resolution near or below 1%.

In order to study the influence of bremsstrahlung at other geometries we display in Fig. 7 photon angular distributions at two scattering angles in the backward hemi-

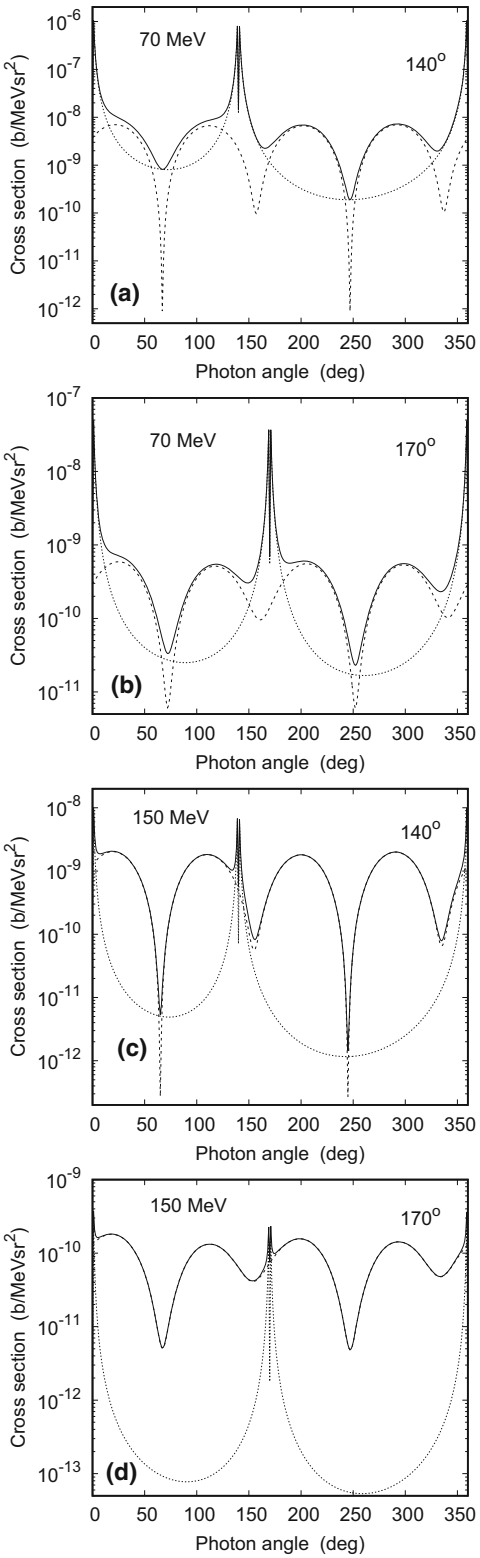

Fig. 7 Averaged triply differential cross section for the coincident $(e, e'\gamma)$ process by **a**, **b** 70 MeV and **c**, **d** 150 MeV electrons as a function of photon angle θ_k. The scattering angle is **a**, **c** $\vartheta_f = 140°$ and **b**, **d** $\vartheta_f = 170°$, at $\varphi = 0$. The detector resolution is $\Delta\omega/\omega = 3\%$. Dashed line – Photons from the nuclear ExDec process; dotted line – bremsstrahlung; full line – coherent sum

sphere, $\vartheta_f = 140°$ and 170°, and two collision energies, 70 MeV and 150 MeV. In all subfigures, an average is taken with $\Delta\omega/\omega = 3\%$. Comparing Figs. 6a, 7a, b, it is seen that, away from the bremsstrahlung peaks, the influence of bremsstrahlung decreases with scattering angle, favouring the backmost angles. Also, profiting from a weak dependence of the nuclear ExDec process on collision energy [11], while bremsstrahlung is strongly decreasing with E_e, bremsstrahlung is the more suppressed, the higher E_e, see Fig. 7c, d.

3 Polarized electrons

Previous investigations of the ExDec process were restricted to unpolarized beam electrons. However, a new set-up has been installed at the S-DALINAC which allows for experiments with polarized beams [27]. Also at the Mainz Microtron (MAMI) it is planned to collide polarized electrons with ^{12}C in the context of parity violation investigations. In fact, a more stringent test of the nuclear models is achieved if additionally the spin degrees of freedom are taken into account. An appropriate measure of the spin asymmetry is the Sherman function S [28,29] which requires a beam polarization perpendicular to the scattering plane. It measures the relative difference in intensity when the direction of the beam polarization is switched.

In the discussion of the spin asymmetry we will disregard bremsstrahlung, since actual measurements will always be performed at photon angles where the influence of bremsstrahlung is small. In that case, the Sherman function can alternatively be obtained from the transition amplitude $M_{fi}^{(1)}$. Denoting the coefficients of the initial-state polarization vector $\boldsymbol{\zeta}_i$ in the standard basis $\binom{1}{0}$ and $\binom{0}{1}$ by a_{m_i}, $M_{fi}^{(1)}$ is formally written as [18]

$$M_{fi}^{(1)} = \sum_{m_i=\pm\frac{1}{2}} a_{m_i}\, F(m_i), \tag{3.1}$$

and the Sherman function results from [20]

$$S = -2\,\frac{\sum_\lambda \mathrm{Im}\,\{F^*(\frac{1}{2})\cdot F(-\frac{1}{2})\}}{\sum_\lambda\left[\left|F\left(\frac{1}{2}\right)\right|^2 + \left|F\left(-\frac{1}{2}\right)\right|^2\right]}. \tag{3.2}$$

The denominator is proportional to the total cross section for unpolarized particles, obtained by summing (in addition to m_i) over the two photon polarizations $\boldsymbol{\epsilon}_\lambda$ and over the projections of the two spin polarization vectors $\boldsymbol{\zeta}_f$ of the final electron (note, however, that $F(m_i)$ is independent of σ_f if $\boldsymbol{\zeta}_f$ is taken parallel, respectively, antiparallel to $\boldsymbol{k}_f$).

Figure 8 provides examples for the spin asymmetry in case of some geometries from Fig. 7. The total cross section being in the denominator of (3.2), S has extrema at photon angles where the minima of the cross section are located (see also Fig. 9). In the forward hemisphere, and even at scattering angles up to 140°, the cross section has very deep minima and consequently, the maxima of S are very sharp. In a true experimental situation the excursions of S at such angles will be reduced since bremsstrahlung tends to fill the cross section minima. At the backmost scattering angles, diffraction effects come into play and modulate the sign of S. Such diffraction effects occur when the electron is sufficiently energetic to penetrate the nuclear surface and to scatter off the individual protons.

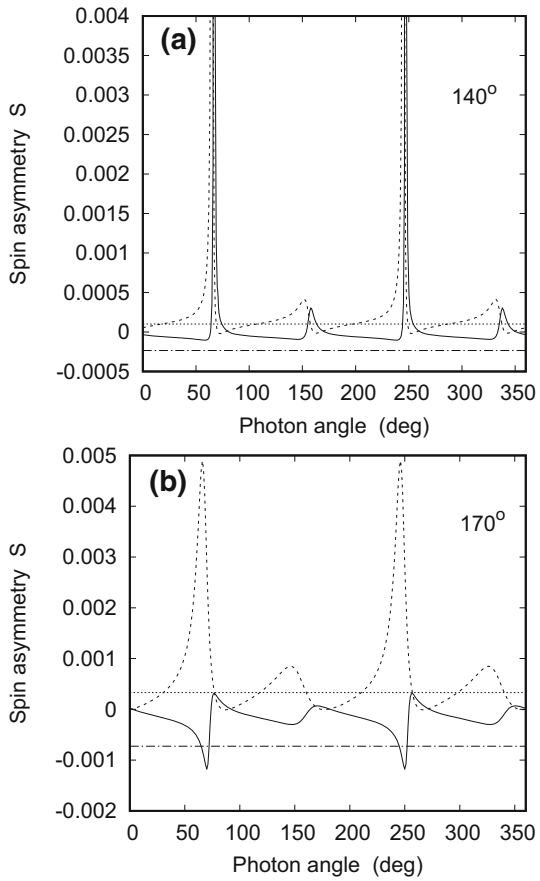

Fig. 8 Spin asymmetry for the nuclear ExDec process from the carbon 2_1^+ excitation by 70 MeV (full line) and 150 MeV (dashed line) perpendicularly polarized electrons as a function of photon angle θ_k for scattering angles **a** $\vartheta_f = 140°$ and **b** $\vartheta_f = 170°$ at $\varphi = 0$. The maxima of S in **a** amount to 0.031 for 70 MeV and to 0.066 for 150 MeV (using a step size of $\Delta\theta_k = 1°$ in the plot). Also shown is the spin asymmetry from the excitation process alone (dash-dotted line – 70 MeV; dotted line – 150 MeV)

In Fig. 8 we have included the spin asymmetry resulting from the mere excitation process as full line. It is calculated by replacing $M_{fi}^{(1)}$ with the amplitude A_{ni}^{exc}, for which an equation of type (3.1) also holds. In (3.2), the sum over λ has to be changed into a sum over M_n [20]. For excitation it is well known (and verified in Fig. 8) that $|S|$ decreases globally with E_i (at fixed ϑ_f) and increases with scattering

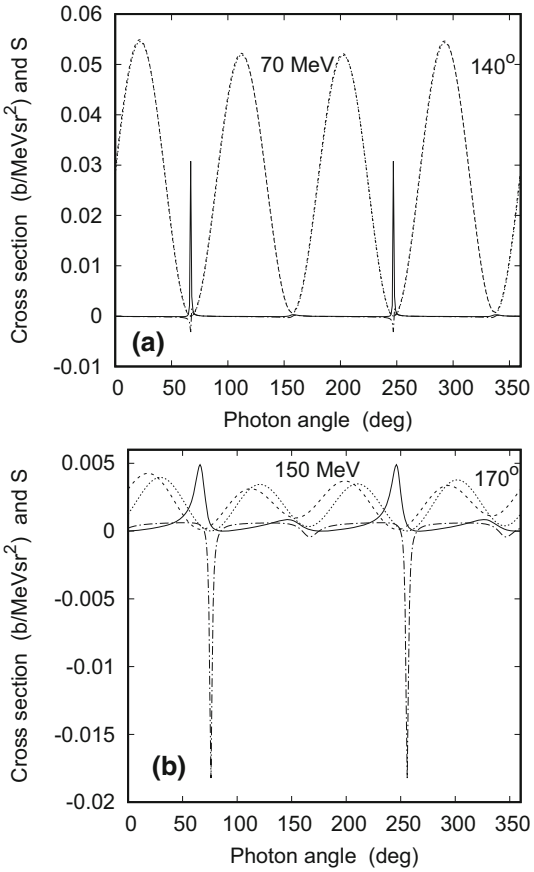

Fig. 9 Spin asymmetry for nuclear excitation and decay of the ^{12}C, 2^+_1 state by perpendicularly polarized electrons of **a** 70 MeV at $\vartheta_f = 140°$ and **b** 150 MeV at $\vartheta_f = 170°$, with $\varphi = 0$, as a function of photon angle θ_k. Shown is S from the nuclear ExDec process using the QPM densities (full line) and the Ravenhall densities (dash-dotted line). Also shown is the corresponding (unaveraged) triply differential cross section (in $\frac{b}{MeVsr^2}$) from the QPM densities (dashed line) and from the Ravenhall densities (dotted line). In **a**, the Ravenhall cross section is scaled down by a factor of 0.26, in **b** the QPM cross section is scaled up by a factor of 3 to display the differences in shape

angle (at fixed E_i). It is only the latter fact which remains true for the nuclear ExDec process.

In order to demonstrate the greater sensitivity of S to the choice of nuclear models as compared to the perceptivity of the cross section for unpolarized particles, we display in Fig. 9 the results obtained from the QPM transition densities on the one hand, and from the Ravenhall transition densities on the other hand. At a beam energy of 70 MeV and $\vartheta_f = 140°$ (Fig. 9a) the Ravenhall cross section is by a factor of 3.85 higher, but the shape of the angular distribution is nearly identical. The Sherman function, however, differs visibly. In particular, the maxima in S from the QPM prescription have turned into weak minima in the Ravenhall picture. The sensitivity to details in the transition densities increases with energy. In Fig. 9b a collision energy of 150 MeV is chosen, together with a backward scattering angle of 170° which increases the spin asymmetry in the regions between the sharp peaks considerably. In this geometry, the Ravenhall cross section is enhanced by a factor of 3, and the angular distribution is slightly modulated and shifted. The Sherman function, on the other hand, shows considerable deviations in the two prescriptions. The maxima of the QPM model have now turned into deep minima. These extrema are nevertheless wide enough to make a detection feasible. Moreover, as becomes clear from a comparison with Fig. 7d, bremsstrahlung plays no role except in a small region around $\theta_k = 170°$, so that the extrema in S are not influenced.

4 Conclusion

We have calculated the triply differential cross section for the simultaneous observation of the scattered electron and the emitted photon in the $(e, e'\gamma)^{12}$C reaction. The nuclear quasiparticle phonon model was used for the excitation of the 2^+_1 state, while electron scattering was described within the distorted-wave Born approximation. Comparing with earlier results using experimental nuclear transition densities, large changes in the photon intensity are found, but only slight shifts of the angular distribution, even at backward scattering angles. The measured relative photon distribution is well reproduced in both prescriptions.

Confirming earlier results on quadrupole excitation of ^{92}Zr, the M_n-sublevels of the ^{12}C, 2^+_1 excited state are approximately equally populated for scattering angles in the forward hemisphere, while the $M_n = 0$ and $M_n = 1$ substates largely dominate at the backmost angles. Consequently, at the smaller angles the photon angular distribution has a regular quadrupole structure, while there are substantial dipole-type modifications (from the $M_n = 1$ contribution) at scattering angles close to 180°.

Including bremsstrahlung within the PWBA, a theory well justified for low-energy photons and a light nucleus like ^{12}C even for large scattering angles, it was found that for photon angles in the forward direction or close to the scattering angle, bremsstrahlung spoils the visibility of the nuclear decay photons, the more so, the smaller the scattering angle, the lower the collision energy and the poorer the resolution of the photon detector.

Finally we have investigated the Sherman function which is a measure of the spin asymmetry occurring for polarized electron impact. In contrast to its behaviour for elastic scattering or excitation where the spin asymmetry exhibits a global decrease with collision energy (which may be modulated by diffraction structures), the ExDec process will lead to considerably higher spin asymmetries when E_e is increased. Furthermore, by comparing the results from the two considered types of nuclear transition densities, we have demonstrated that the Sherman function is much more sensitive to such

changes than the triply differential cross section. The large deviations of S in the two models at high collision energies, combined with its high absolute values at the backmost scattering angles where the influence of bremsstrahlung is negligible, make such a geometry a promising candidate for nuclear structure investigations.

Acknowledgements Open Access funding provided by Projekt DEAL. V.Yu. P. acknowledges support by the Deutsche Forschungsgemeinschaft (DFG, German Research Foundation) – Projektnummer 279384907-SFB 1245.

Data Availability Statement This manuscript has no associated data or the data will not be deposited. [Authors' comment: No data exist beyond those contained in the figures.]

References

1. C.N. Papanicolas et al., Phys. Rev. Lett. **54**, 26 (1985)
2. D.G. Ravenhall, R.L. Schult, J. Wambach, C.N. Papanicolas, S.E. Williamson, Ann. Phys. **178**, 187 (1987)
3. H. Überall, *Electron Scattering from Complex Nuclei* (Academic Press, New York, 1971)
4. J. Heisenberg, H.P. Blok, Ann. Rev. Nucl. Part. Sci. **33**, 569 (1983)
5. D.F. Hubbard, M.E. Rose, Nucl. Phys. **84**, 337 (1966)
6. H.L. Acker, M.E. Rose, Ann. Phys. **44**, 336 (1967)
7. H.L. Crannell, Phys. Rev. **148**, 1107 (1966)
8. J.B. Flanz, R.S. Hicks, R.A. Lindgren, G.A. Peterson, A. Hotta, B. Parker, R.C. York, Phys. Rev. Lett. **41**, 1643 (1978)
9. H. Bethe, W. Heitler, Proc. R. Soc. (Lond.) A **146**, 83 (1934)
10. H.A. Bethe, L.C. Maximon, Phys. Rev. **93**, 768 (1954)
11. D.H. Jakubassa-Amundsen, V.Yu. Ponomarev, Phys. Rev. C **95**, 024310 (2017)
12. *Atomkerne: Von fundamentalen Wechselwirkungen zu Struktur und Sternen*, Deutsche Forschungsgemeinschaft (DFG, German Research Foundation) – Projektnummer 279384907-SFB 1245
13. V.G. Soloviev, *Theory of Atomic Nuclei: Quasiparticles and Phonons* (Institute of Physics, Bristol, 1992)
14. N. Lo Iudice, V.Yu. Ponomarev, Ch. Stoyanov, A.V. Sushkov, V.V. Voronov, J. Phys. G **39**, 043101 (2012)
15. E.S. Ginsberg, R.H. Pratt, Phys. Rev. **134**, B773 (1964)
16. D.H. Jakubassa-Amundsen, Phys. Lett. A **377**, 1885 (2013)
17. S.T. Tuan, L.E. Wright, D.S. Onley, Nucl. Instr. Meth. **60**, 70 (1968)
18. E.M. Rose, *Relativistic Electron Theory* (Wiley, New York, 1961), §15–19
19. S. Raman, C.W. Nestor, Jr., P. Tikkanen, At. Data Nucl. Data Tables **78**, 1 (2001)
20. D.H. Jakubassa-Amundsen, Nucl. Phys. A **937**, 65 (2015)
21. F. Salvat, J.M. Fernández-Varea, W. Williamson Jr., Comput. Phys. Commun. **90**, 151 (1995)
22. H. De Vries, C.W. De Jager, C. De Vries, At. Data Nucl. Data Tables **36**, 495 (1987)
23. C.M. Vincent, H.T. Fortune, Phys. Rev. C **2**, 782 (1970)
24. D.H. Jakubassa-Amundsen, V.Yu. Ponomarev, Eur. Phys. J. A **52**, 48 (2016)
25. F. Ajzenberg-Selove, C.L. Busch, Nucl. Phys. A **336**, 1 (1980)
26. A. Lovato, S. Gandolfi, J. Carlson, S.C. Pieper, R. Schiavilla, Phys. Rev. Lett. **117**, 082501 (2016)
27. Y. Poltoratska et al., AIP Conf. Proc. **1149**, 715 (2009)
28. N. Sherman, Phys. Rev. **103**, 1601 (1956)
29. J.W. Motz, H. Olsen, H.W. Koch, Rev. Mod. Phys. **36**, 881 (1964)